International Journal for Numerical Methods in Fluids

VERIFICATION AND VALIDATION OF NUMERICAL SOLUTIONS OF TWO-DIMENSIONAL REACTIVE FLOW IN ROCKET ENGINE NOZZLES

Journal:	*International Journal for Numerical Methods in Fluids*
Manuscript ID:	Draft
Wiley - Manuscript type:	Research Article
Date Submitted by the Author:	n/a
Complete List of Authors:	Araki, Luciano; Federal University of Parana, Mechanical Engineering Marchi, Carlos; Federal University of Parana, Mechanical Engineering
Keywords:	Finite volume method, Non-orthogonal grid, LOX/LH2, Numerical error estimate, Verification, Nozzle

VERIFICATION AND VALIDATION OF NUMERICAL SOLUTIONS OF TWO-DIMENSIONAL REACTIVE FLOW IN ROCKET ENGINE NOZZLES

L. K. Araki, C. H. Marchi

Federal University of Paraná (UFPR), Department of Mechanical Engineering (DEMEC). 81531-980, Curitiba - Pr, Brazil. E-mails: lucaraki@ufpr.br, marchi@ufpr.br

ABSTRACT

Two-dimensional mathematical models for LOX-LH_2 reactive flows are solved for a conical and a parabolical geometry. Five different physical models are studied: two one-species and three multi-species ones (frozen, equilibrium and non-equilibrium flows). In the mathematical model, temperature is used as unknown at the energy equation and velocity is obtained for all speed flows. For all the analysis, a non-orthogonal finite volume code was implemented, taking into account first (UDS) or second (CDS) order interpolation schemes and co-located grid arrangement. The code validation was provided by the comparison between experimental and numerical results for the conical geometry, which provided good concordance, using grids as refined as 720x80 volumes. For the parabolical geometry, both apparent and asymptotic orders are provided for grids as refined as 640x192 volumes. The apparent order was well-behaved for almost all cases using the UDS scheme, with a clearly tendency to the asymptotic order. On the other hand, when CDS was used, the observed tendency was unclear in some cases. Numerical solutions, including their error estimates, are provided for UDS and CDS schemes. An analysis of them shows that global variables of interest (such as thrust and specific impulse) are smaller affected by the chosen physical model than local variables of interest (such as the temperature at line symmetry).

Keywords: Finite Volume Method, Non-Orthogonal Grid, LOX-LH_2, Numerical Error Estimate, Verification, Nozzle.

SHORT TITLE: V&V of Numerical Solutions of 2-D Reactive Flows in Rocket Nozzles

1. INTRODUCTION

The effort to increase reliability in rocket engines should span the entire program spectrum from conceptual design through production. The reliability effort can basically be split into three parts: prevention of failures, process assessment and control, and monitoring of performance [1]. One important reason of the wall material failure is the high temperatures achieved and this is the major reason for studies involving the heat transfer overall the rocket engine nozzle. In order to study the heat transfer phenomena, otherwise, it is essential to be familiar with aspects related to the reactive gas flow through the entire nozzle.

Many papers about heat transfer and reactive gas flow in rocket engine nozzles have been published in the last years, including: fluid-structure interactions in regenerative cooling systems [2]; reactive gas flow and regenerative cooling system [3]; two- and three-dimensional turbulent flows and radiative heat transfer [4]; liquid film cooling effects [5]; and the startup side load analysis in a regeneratively cooled nozzle [6]. Although some of these works are concerned about numerical validation, including comparisons between numerical results and experimental data, none of them brings numerical verification results.

Unfortunately, the numerical error analysis for supersonic flows is not a common practise: none of the studies cited before employed numerical tools for providing numerical error estimates, neither a study about the orders of numerical error. It may be related to the fact that the theoretical foundation of a posteriori and a priori error analysis is far from satisfactory for nonlinear hyperbolic problems, such as supersonic flows. Moreover, despite its importance in pratical applications, only recently the difficulties in estimating the errors and its control have received more attention [7].

According to Oberkampf and Trucano [8], verification and validation are the primary means to assess the accuracy and reliability of computational simulations. While validation is associated with the accurateness of a mathematical model in relation to a real physical phenomenon, verification consists on the quantification of the numerical error [9-10].

Therefore, the purposes of the current work are: (1) to validate a numerical code for two-dimensional compressible reactive and non-reactive flows; (2) to provide a posteriori error analyses for reactive compressible flows, by the comparison between the asymptotic and the aparent orders and also the GCI numerical error estimates [11]; and (3) to compare the performance of six and eight species models for chemical reaction schemes, for both rocket engine parameters and the CPU time requirements.

In order to achieve these previously cited aims, the numerical model includes: the Finite Volume Method [12], co-located non-orthogonal grids, all speed flow methodology [13], temperature as variable at the energy equation and different physical models (for one and multi-species flows, which contains a range of chemical reaction schemes). The implemented code also allows the use of the following interpolation schemes: UDS, CDS with deffered correction [14], or even a hybrid scheme. Although the steady flow regime is the desired one, time is used, in a totally implicit form, as relaxation parameter.

The adopted numerical method allows the achievement of all the flow regimes into the rocket nozzle engine (sub-, trans- and supersonic ones), differently from the commonly used method of characteristics [15-16], which can be used only for hyperbolic problems (correspondent to supersonic flows). And differently from the MacCormack's method, which is also widely used for nozzle flow studies [15], the implemented code presents a totally implicit methodology, and not an explicit one.

The adopted mathematical model is presented in Section 2, while details of the discretization and the used algorithm are given in Section 3. Some basic information about verification is presented in Section 4, while the geometry, the boundary conditions and associated information is exposed in Section 5. Numerical results and their discussion are provided in Section 6 and the final remarks are exposed in Section 7.

2. MATHEMATICAL MODEL

The basic principles involved in rocket propulsion science are essentially those ones of mechanics, thermodynamics and chemistry [17]. In regeneratively cooled rocket engines, the whole thrust mechanism can be split into three different (but coupled) problems, for which there are independent mathematical (and numerical) models [18-20]: (1) the reaction gas products (combustion gases mixture) flow through the thrust chamber; (2) the heat conduction from hot gases to the coolant; and (3) the coolant flow through the regenerative cooling system. The focus of this work is, however, only the reaction gas products flow, which can be modelled by the mass conservation, two-dimensional (axial and radial) Euler and energy equations, and a state relation, as follows:

$$\frac{\partial}{\partial z}(\rho u)+\frac{1}{r}\frac{\partial}{\partial r}(r\rho v)=0 \tag{1}$$

$$\frac{\partial}{\partial z}(\rho u u)+\frac{1}{r}\frac{\partial}{\partial r}(r\rho v u)=-\frac{\partial P}{\partial z} \tag{2}$$

$$\frac{\partial}{\partial z}(\rho u v)+\frac{1}{r}\frac{\partial}{\partial r}(r\rho v v)=-\frac{\partial P}{\partial r} \tag{3}$$

$$\frac{\partial}{\partial z}(\rho u T)+\frac{1}{r}\frac{\partial}{\partial r}(r\rho v T)=\frac{1}{c_p}\left[\nabla(P\mathbf{V})-P\nabla\mathbf{V}\right]+S_{eq/ne} \tag{4}$$

$$P=\rho R T \tag{5}$$

where: ρ, u, v, P and T are the five dependent variables, which correspond to density, axial and radial velocity components, pressure and temperature, respectively; z and r are related to the axial and the radial directions, in this order; c_p is the frozen specific heat; R is the one-species constant or multi-species mixture constant; $\mathbf{V}$ is the velocity vector; and $S_{eq/ne}$ is the chemical source term, which is null for all the cases, excepted by local equilibrium flow model, for which it is evaluated by:

$$S_{eq/ne}=-\frac{1}{c_p}\left[\sum_{i=1}^{N}h_i\frac{\partial}{\partial z}(\rho u Y_i)-\sum_{i=1}^{N}h_i\frac{1}{r}\frac{\partial}{\partial r}(r\rho v Y_i)\right] \tag{6a}$$

and by non-equilibrium flow model, for which it is estimated by:

$$S_{eq/ne}=-\frac{1}{c_p}\sum_{i=1}^{N}h_i\dot{w}_i \tag{6b}$$

In Eq. (6), N is the total number of chemical species; Y_i, h_i and $\dot{w}_i$ are, in this order, the mass fraction, the enthalpy and the generation rate for a given chemical species i. Considering the non-equilibrium flow, another equation must be taken into account: the species continuity equation,

$$\frac{\partial}{\partial z}(\rho u Y_i)+\frac{1}{r}\frac{\partial}{\partial r}(r\rho v Y_i)=\dot{w}_i \tag{7}$$

The chemical reaction schemes used in this work for frozen and local equilibrium flows are summarized in Tab. 1. For non-equilibrium one, only six and eight reaction scheme models were considered, being the frozen/equilibrium chemical model 3 split into two: models 31 and 32, which differs from each other by forward reaction constants. These are the same chemical reaction schemes previously used [25-26], which present, in this order, the thermochemical properties for oxygen/hydrogen reaction schemes and the complete one-dimensional problem.

[Table 1]

3. NUMERICAL MODEL

The presented mathematical model for reaction gas products is discretized using the Finite Volume Method [12] for non-orthogonal grids. The domain is divided in *Nz* control volumes in axial direction *z* and in *Nr* volumes in radial direction *r*, in which the differential equations are integrated. A co-located grid arrangement, as well as a formulation for all speed flows [13], is used, associated to a first-order (UDS), a second-order (CDS), or a hybrid order (between UDS and CDS) interpolation scheme; for the second-order, so as to allow a better convergence, deferred correction [14] was employed. The systems of algebraic equations obtained by the discretization process are solved by the MSI (Modified Strong Implicit) method [27].

Pressure and velocity are coupled by the SIMPLEC algorithm [28], in order to convert the mass equation in a pressure (or better, in a pressure-correction) one. So, the mass conservation equation, Eq. (1), is used for determination of a pressure-correction (P'). The axial and radial velocity components, (u) and (v), are obtained from the Euler equations, Eqs. (2) and (3), and the energy equation, Eq. (4), is taken for temperature (T) determination. Density (ρ) is gotten from the state equation, Eq. (5), while Eq. (7) is also needed for the non-equilibrium flow. It must be noted that the axial velocity (u) is evaluated from reduced (near null) values until supersonic ones, and not only for supersonic values, as commonly found in literature for the method of characteristics.

An algorithm for the reactive two-dimensional reaction gas products flow is presented in the following.

3.1. Algorithm:

1. Data reading, grid generation and evaluation of metrics.
2. Estimation of all variables in an instant t+Δt (time, however, is only used as a relaxation parameter).
3. Estimation of the inlet pressure and the inlet temperature; definition of the frozen constant-pressure specific heat.
4. Coefficients evaluation for the algebraic system (by discretization) of the axial momentum equation and solution of this system by MSI for the axial velocity component u.
5. Coefficients evaluation for the algebraic system (by discretization) of the radial momentum equation and solution of this system by MSI for the radial velocity component v.
6. Coefficients evaluation for the algebraic system (by discretization) of the energy equation and solution by MSI for temperature T.
7. Calculation of density (both, inside the control volumes and at their faces), SIMPLEC coefficients and estimation of face velocities.
8. Coefficients evaluation for the algebraic system (by discretization) of the mass equation and solution by MSI for pressure correction P'.
9. Correction of nodal pressures, face and nodal densities, and face and nodal velocities by pressure correction P'.
10. Return to item 8 until the achievement of the desired number of iterations.
11. In case of non-equilibrium flow model, the mass fractions Y_i should be obtained by the solution of an algebraic system using the MSI method.

12. Return to item 2, until the achievement of the desired number of iterations or until the satisfaction of a criterion (maximum number of interations or tolerance).
13. Post-processing.

4. NUMERICAL ERROR ANALYSIS

While the asymptotic (expected) convergence order, p_L, is evaluated based on the Taylor Series analyses of the numerical interpolation schemes employed in the mathematical model discretization, to estimate the apparent convergence order, p_U [29], three numerical solutions, φ_1, φ_2 and φ_3, are needed. These solutions are related to three different grids, named, respectively, as fine (h_1), coarse (h_2) and supercoarse (h_3), where *h* is the average volume size for the used grid. Thus, the obtained relation is:

$$p_U(h_1) = \frac{\log\left[\frac{(\varphi_2 - \varphi_3)}{(\varphi_1 - \varphi_2)}\right]}{\log(q)} \tag{8}$$

where *q* is the grid refinement ratio, taken as constant for all the three grids, defined as

$$q = \frac{h_2}{h_1} = \frac{h_3}{h_2} \tag{9}$$

Both asymptotic and apparent convergence orders are important for the evaluation of the GCI estimator [11] and the Richardson estimator [30-31], given by the following relations, respectively:

$$GCI(\varphi_1, p) = 3\frac{|\varphi_1 - \varphi_2|}{(q^p - 1)} \tag{10}$$

and

$$U_{Ri}(\varphi_1, p) = \frac{(\varphi_1 - \varphi_2)}{(q^p - 1)} \tag{11}$$

where *p* assumes the lowest value between p_L or p_U for the GCI estimator, and it can be either p_L or p_U, if the interest is on asymptotic or on apparent order, for the Richardson estimator.

5. DEFINITION OF THE PROBLEM

The boundary conditions for the combustion gases flow, applied with ghost-cells, are:

- Entrance conditions: temperature (*T*) and pressure (*P*) are functions of the stagnation parameters; the chemical mixture composition, given by mass fractions (Y_i), is obtained from local data (temperature and pressure); this last item is not necessary for one-species models. The entrance axial velocity (*u*) is obtained from a linear extrapolation from the values obtained for internal flow. The radial velocity (*v*) is null.
- Nozzle walls: adiabatic.
- Exit conditions: for supersonic flows in nozzles, no exit boundary conditions are required; for the implementation of a numerical model, however, exit boundary conditions are needed.

Because of this, temperature (T), axial and radial velocities (u and v), pressure (P) and mass fractions (Y_i) are obtained by linear extrapolation from internal control volumes.

- Line symmetry: symmetry conditions for all variables; null radial velocity.

For all the simulations, two different geometries were chosen (shown at Fig. 1): the first one is presented by Back et al. [32]; and the second one is a parabolic nozzle.

[Figure 1]

The global parameters of interest in this work are the nozzle discharge coefficient (C_d), the thrust for vacuum conditions (F) and the specific impulse (I_s), which are defined by

$$C_d = \frac{\dot{m}_{\exp}}{\dot{m}_{theor}}; \qquad F = \int_{S_{ex}} \rho u^2 \, dS; \qquad I_s = \frac{\int_0^{tb} F \, dt}{g \int_0^{tb} \dot{m}_p \, dt} \tag{12}$$

where $\dot{m}_{\exp}$ is the numerical result for mass flow rate at nozzle, $\dot{m}_{theor}$ is the isentropic one-dimensional mass flow rate for the same nozzle conditions, S_{ex} is the cross-section area at the nozzle exit, g is the gravitational acceleration, $\dot{m}_p$ is the propellant mass flow rate and tb is the propellant burn-out time.

6. NUMERICAL RESULTS AND DISCUSSION

6.1. Problem 1: Back et al. [32] geometry – Code validation and verification.

For the validation of the implemented code, experimental data provided by Back et al. [32] were employed. In this case, air was modelled as a one-species perfect gas, with the gas constan R = 287.0 J/kg·K and ratio between specific heats, γ = 1.35. Furthermore, the other parameters/properties are: stagnation pressure of 1.725 MPa; stagnation temperature of 833.33 K; CDS interpolation scheme with deferred correction; 90x10, 180x20, 360x40 and 720x80 control volume grids (axial x radial number of volumes); and a number of iterations enough to achieve the machine round-off error. Besides the constant air properties flow, also variable properties ones were studied and both results (constant and variable properties), for a 720x80 control volumes grid, are exposed in Fig. 2. When the one-species variable properties model is employed, the values of the specific heat at constant pressure (c_p) are dependent on the temperature, according to a polynomial fitting obtained by the use of tabulated data provided by Incropera et al. [33]. Comparing numerical to experimental pressure data, a good agreement between both results was observed, which allows the validation of the implemented code.

[Figure 2]

Another validation test for the implemented code was done for the same conical geometry. The experimental data, however, were the ones provided by Cuffel et al. [34] for Mach number at the wall and centerline (symmetry line) of the rocket engine nozzle. In this case, air was modelled as a one-species perfect gas, with ratio between specific heats, γ = 1.40. The stagnation pressure and temperature presented values of, respectively, 482.6 kPa and 300 K. The other numerical parameters were kept equal to the previous validation case. As can be seen at Fig. 3, there is a good concordance between numerical and experimental data for the evaluated Mach number at the nozzle line symmetry. The analytical Mach number over the line symmetry, at the nozzle throat, provided by Kliegel and Levine [35], was also included in Fig. 3: this analytical solution slightly overpredicts both numerical and experimental data.

In the wall vicinity, otherwise, numerical and experimental data concordance is not so good. As exposed by Cuffel et al. [34], experimental data were obtained with a minimum distance of about 1.8 mm from the nozzle wall and, because of this, two sets of numerical results are provided at Fig. 3: one correspondent to the Mach values exactly placed at the nozzle wall and the other one at a distance of 1.8 mm from the wall. Apparently, near-to-wall numerical results underpredict the experimental behaviour, especially in the region between -5 and +5mm around the nozzle throat. It must be noted, however, that experimental data also presents uncertainties and the evaluation of the Mach number is based actually on pressure measurements. As observed by Cuffel et al. [34], the true static pressure could be measured only when the flow was parallel to the used pitot-tube; at some locations, however, the flow was inclined to the tube. In this case, the pressure measured was lower than the true static pressure and a higher-than-true Mach number was calculated [34]. This could be the case of the Mach number at the near-to-wall region, especially around the nozzle throat, once it is the region in which the streamlines continually change their direction. Finally, comparing the numerical results and the experimental data to the analytical Mach number for the nozzle wall, at the nozzle throat, it can be seen that the solution provided by Kliegel and Levine [35] underpredicts both the numerical and experimental results, differently than the exposed behaviour to the nozzle centerline (line symmetry).

[Figure 3]

A third validation test was made taking into account the Mach isolines, obtained for the throat region, using the previous test configuration. In this case, experimental data were the ones also provided by Cuffel et al [34] and are exposed with numerical results for the UDS and CDS interpolation schemes in Fig. 4. As can be seen, both schemes present good concordance with experimental data, especially at the line simmetry. The sonic line is correctly capture by both interpolation schemes and both schemes also capture the weak oblique shock wave formation, although the UDS scheme tends to smooth this region by its diffusive behaviour. The differences between the two interpolation schemes (UDS and CDS) are only more evident for the near-to-wall region and for higher Mach numbers. In the subsonic region, both schemes present almost the same Mach profiles; only for the shock wave downstream region, more significant differences are noticeable and, in general, CDS results present a better agreement to the experimental data.

[Figure 4]

Numerical error estimates, based on the GCI estimator, for the discharge coefficient were also analysed for both constant and variable air flows, and the results are summarized in Tab. 2. As can be seen, numerical results for UDS interpolation scheme, with respective numerical error ranges, enclose those obtained using CDS scheme, as expected, once UDS presents first-order convergence rate, while CDS shows second-order. However, it must be observed that the results for CDS one-species with constant properties do not enclosure the analytical solution provided by Kliegel and Levine [35], which was obtained for an irrotational perfect gas flow, using toroidal coordinates. The differences among both results could be related to the adopted model: for the numerical code, Euler equations for axysimmetric coordinates were employed.

Furthermore, despite the use of four different grids in both presented cases, only one apparent order could be evaluated, based on the triplet 180x20, 360x40 and 720x80 grids, for the CDS scheme. The obtained values were: for the first case, $p_U \approx 2.74$ for one-species, constant properties and $p_U \approx 2.93$ for one-species, variable properties, while for the second case, $p_U \approx 2.29$ for constant properties and $p_U \approx 2.28$ for variable properties; the asymptotic value, for all cases, was $p_L = 2$. On the other hand, the use of the same four grids allows the evaluation of two values for the apparent order, when the UDS scheme was employed; besides, the values of

them are clearly close to the expected one, with $p_U \approx 0.93$ (or $p_U \approx 0.92$), for both physical models, in the finest grid.

The knowledge of only one value for the apparent order for the CDS scheme, although not too far from the asymptotic one, is not enough to assure that the apparent order converges monotonically to the expected/asymptotic one, in other words, belongs to the convergent interval [36], as required by the Richardson and/or the GCI estimator. In cases in which the convergent interval is not observed, error estimators, as the GCI, might result in inaccurate estimates, as discussed by Roache [37]. The comparison among numerical and analytical results and the experimental data for the second case, however, shows that both numerical and analytical results present a good agreement to the experimental data, what can provide another validation result.

[Table 2]

In order to provide a better verification study for Back et al. [32] geometry, additional simulations were also made for multi-species flows. For these studies, the stagnation pressure and temperature were equal to, respectively, 3420.33 K and 2.0 MPa; the oxidant-ful mass ratio (*OF*) was taken as 7.936682739 (which corresponds to the stoichoimetrical composition for the oxygen/hydrogen reaction); the gas constant (*R*) was considered to be 526.97 J/ kg·K; and the ratio ratio between specific heats (γ) was equal to 1.1956 (used for constant properties one-species flow).

Two-dimensional flow effects are qualitatively evident by comparing any property distribution at the line symmetry and in the vicinity of the walls, as can be seen at Fig. 5, for the temperature distribution in different grids. In order to provide a better comparison, the one-dimensional solution for the 720 volumes grid is also presented in Fig. 5. It can also be seen that discrepancies among near-to-wall results are much smaller than the ones obtained for the line symmetry, taking into account the grid refinement. Although Fig. 5 (a) shows only this effect on the temperature distribution, other local variables of interest (such as pressure, Mach number and density distributions) exhibit a qualitatively similar behaviour.

[Figure 5]

6.2. Problem 2. Parabolic nozzle – Numerical verification.

The second geometry employed was the parabolic one, presented in Fig. 1 (b). Numerical results for at least 6 grids were obtained for each chemical/physical model, in order to evaluate the apparent order and the error estimates (by GCI and Richardson estimators). Also both UDS and CDS with deferred correction schemes were employed to study the influence of the chosen interpolation scheme on the error estimate. The number of iterations used was enough to assure the achievement of the machine round-off error. Besides, for both frozen and local equilibrium flow models, the tolerances associated to chemical reactions were posed as 10^{-12} for the chemical dissociation rates, with the purpose of assuring the convergence for the chemical reaction equations. Both frozen and local equilibrium flows are limit cases of the real reactive flow into a rocket nozzle engine [15,16]: while in the former model, the chemical reactions are much faster than the flow speed and, because of this, the chemical composition is kept unchanged along all the flow, for the latter model, the reactions speed tends to infinity and, because of this, chemical equilibrium is achieved for each control volume of the flow. The apparent order behaviour, for global variables of interest, is shown in Fig. 6, while the error estimate, for the specific impulse (I_S) is placed in Fig. 7. Both results refer to chemical model 4, for frozen flow and 10x3, 20x6, 40x12, 80x24, 160x48, 320x96 and 640x192 control volume grids.

[Figure 6]

According to Fig. 6, the apparent order tends to the asymptotic one for UDS, while, to the same grids, when CDS is used, this tendency is yet unclear. This behaviour was observed not only for the specific impulse but also for all the other global variables of interest for the frozen flow model. Otherwise, local variables of interest (such as the exit temperature at the line symmetry) have unclear tendency even for the UDS scheme. Such behaviour might be associated both to the chemical reaction and to the variations on the property values, which could cause some instabilities on the convergence tendency of numerical results and, consequently, in apparent order values.

The error estimate for both Richardson and GCI estimators are shown at Fig. 7. Despite the unclear tendency for the apparent orders when CDS scheme is used, numerical error estimates are, at least, three orders-of-magnitude smaller than the ones for UDS scheme, at a 640x192 volumes grid. Based on this, it is recommended to use the CDS scheme, even if no clear tendency to the apparent order is yet observed, due to the smaller values for numerical error estimates for frozen flow.

[Figure 7]

Local equilibrium flow results are presented at Figs. 8 and 9. Differently from the frozen flow model, apparent order has a tendency far from the forecasted value of 2: even if this study is restricted to only 6 grids (10x3, 20x6, 40x12, 80x24, 160x48 and 320x96), both the discharge coefficient and the specific impulse show apparent order values close (or they tend) to the unity. Each term of the five governing equations was discretized using both UDS and CDS with deferred correction schemes, except by the chemical source term – Eq. 6(a). This term was discretized using the UDS scheme and, as can be seen by the numerical results, its inclusion possibly changes the convergence order of the entire model to the unity, even when CDS is employed for all the other terms in the discretization process of the governing equations. However, as initially almost all the discretization components presents second order approximations, the related numerical error, when compared to the pure UDS scheme, is smaller. It influences the behaviour of the numerical error estimates (for example, for thrust and specific impulse) for CDS results, which are still at least one order-of-magnitude smaller than the ones obtained with UDS, as can be seen at Fig. 9.

[Figures 8 and 9]

Tables 3 and 4 provide comparisons of physical and chemical models, as well as interpolation schemes (UDS and CDS with deferred correction). These results include the GCI error estimates, except by the H_2O-exit mass fraction for frozen flow models. The choice of GCI estimator is based on the recommendation of the ASME Standard for Verification and Validation [38]. For the discharge coefficient (C_d), the analytical solution of Kliegel and Levine [35] is also supplied. This solution is based on the hypothesis of a perfect gas flow with constant properties, which matches with the one-species, constant-properties model. Although the results of both function interpolation schemes for the discharge coefficient include the analytical solution taking into account the error estimate ranges, CDS ones are, at least, three orders-of-magnitude smaller than those ones obtained for the UDS scheme. Similar behaviour is observed for all physical and chemical models and for all variables of interest. The advantage of CDS scheme is smaller only for local equilibrium flow model, for which the convergence order tends to the unity value. It should be noted, also, that numerical results, including numerical error ranges, for UDS scheme perfectly enclosures CDS results for all variables of interest, except by thrust employing the equilibrium flow model. For this last case, there is an intersection zone between both results sets, which does not enclosure the whole CDS results set; it might be a consequence of the fact that CDS apparent convergence order do not tend to the value of two, but is degenerated to the unity value.

[Tables 3 and 4]

Based on the numerical results presented in Tab. 3 and 4, and the related error estimates, some comparisons among different physical models are made. To start with, it can be observed that the differences among physical models are relatively small for all global variables of interest: it corresponds only to 9.1% for discharge coefficient, 2.7% for thrust and 9.5% for specific impulse. For local variables, otherwise, these discrepancies are more appreciable: 20.4% for exit pressure and 37.9% for exit temperature (at line symmetry). The axial exit velocity, otherwise, is less influenced by the physical model, once the observed variation between the extreme values is about 8.0%. One interesting remark is that six and eight chemical species models present similar results, which are, for many variables, numerically identical, once the error estimate ranges are the same. This observation, however, is not valid when the CPU time is compared: taking as example the 320x96 grid with CDS scheme for the local equilibrium flow, while model 4 demanded 13.6 hours for 30,000 iterations, model 10 needed 21.3 hours (57.3% more), for the same number of iterations. Considering only the CPU time, however, the non-equilibrium models are the ones which present the highest processing requirements: for example, for the 320x96 grid and UDS scheme, the model 31 simulation lasted 5.92 days (2,000,000 iterations), while model 32 lasted 6.57 days (2,300,000 iterations) to the machine round-off error achievement. All the numerical results were obtained in a PC Pentium IV, 3400 MHz, with 4.0 GB RAM.

7. CONCLUSIONS

Verification and validation of a numerical code for two-dimensional, inviscid, one- or multi-species flows were presented in this paper. Numerical results for air flow through a conical rocket engine nozzle were compared to the experimental data provided by Back et al. [32], for pressure, and by Cuffel et al. [34], for Mach numbers, showing good agreement and validating the code. This conical geometry was also employed to show two-dimension flow effects on thermophysical properties, such as the temperature, providing information about the centre and the near-to-wall numerical results.

For numerical verification, a second geometry was employed: a parabolic one. Apparent convergence order, Richardson and GCI error estimators were obtained for all numerical results, which include first (UDS) and second order (CDS with deferred correction) interpolation schemes and five different physical models. The UDS apparent order tends to the asymptotic one for both frozen and local equilibrium flows, while CDS apparent order does not have a clear tendency for frozen flow (besides it is near the value of two) and appears to degenerate to the unity value for local equilibrium flow. This last result could be attributed to the fact that the source term of the energy equation, related to chemical reactions, was discretized employing the UDS interpolation scheme, and it might change the convergence order of the entire numerical model.

The UDS results, with their corresponding error ranges, enclosure the CDS ones, as expected, apart from the thrust for the local equilibrium model. In this case, there is an intersection set, but as the apparent order of both might tend to the unity value, the sets should not match entirely. The differences for global variables of interest among different physical models are relatively small (under 10%), while the variations are more considerable for local variables (they achieve almost 40% for exit temperature). Other numerical results for both UDS and CDS interpolation schemes, with GCI error estimates, were provided, for various propulsion variables of interest. It was also observed that numerical results for six and eight-species models were numerically equivalent, althout the CPU time requirements of the former model are much smaller.

ACKNOWLEDGEMENTS

The authors would acknowledge the Federal University of Paraná (UFPR), the Department of Mechanical Engineering (DEMEC) and the “UNIESPAÇO Program” of The Brazilian Space Agency (AEB) by physical and financial support given for this work. The first author would, also, grant the support provided by the Laboratory of Numerical Experimentation (LENA), and was

supported by a scholarship of CAPES (Coordenação de Aperfeiçoamento de Pessoal de Nível Superior) – Brazil. The second author is supported by a scholarship of CNPq (Conselho Nacional de Desenvolvimento Científico e Tecnológico) – Brazil.

REFERENCES

1. Huzel D K, Huang DH. *Modern Engineering for Design of Liquid-Propellant Rocket Engines*. AIAA Progress in Astronautics and Aeronautics: Washington, 1992.
2. Kuhl D, Riccius J, Haidn OJ. Thermomechanical analysis and optimization of cryogenic liquid rocket engines. *Journal of Propulsion and Power* 2002; **18**: 835-846.
3. Naraghi MH, Dunn S, Coats D. A model of design and analysis of regeneratively cooled rocket engines. *Proceedings of the Joint Propulsion Conference*, Fort Lauderdale, USA, 2004; AIAA 2004-3852.
4. Wang TS. Multidimensional unstructured-grid liquid rocket-engine nozzle performance and heat transfer analysis. *Journal of Propulsion and Power* 2006; **22**(1): 78-84.
5. Zhang HW, Tao WQ, He YL, Zhang W. Numerical study of liquid film cooling in a rocket combustion chamber. *International Journal of Heat and Mass Transfer* 2006; **49**: 349-358.
6. Wang TS. Transient three-dimensional startup side load analysis of a regeneratively cooled nozzle. *Shock Waves* 2009; **19**: 251-264.
7. Zhang XD, Pelletier D, Trépanier JY, Camarero R. Numerical assessment of error estimators for Euler equations. *AIAA Journal* 2001; **39**: 1706-1715.
8. Oberkampf WL, Trucano TG. Verification and validation benchmarks. *Nuclear Engineering and Design* 2008; **238**: 716-743.
9. Metha UB. Guide to credible computer simulations of fluid flows. *Journal of Propulsion and Power* 1996; **12**(5): 940-948.
10. Roache PJ. *Verification and Validation in Computational Science and Engineeering*. Hermosa Publishers: Albuquerque, 1998.
11. Roache PJ. Persperctive: A method for uniform reporting of grid refinement studies. *Journal of Fluids Engineering* 1994; **116**: 405-413.
12. Versteeg HK, Malalasekera W. *An Introduction to Computational Fluid Dynamics - The Finite Volume Method*, 2 ed. Prentice Hall: Harlow, 2007.
13. Marchi CH., Maliska CR. A nonorthogonal finite volume method for the solution of all speed flows using co-located variables. *Numerical Heat Transfer – Part B* 1994; **26**: 293-311.
14. Ferziger JH, Perić M. *Computational Methods for Fluid Dynamics*, 3ed., Springer-Verlag: Berlin, 2001.
15. Anderson JA. *Modern Compressible Flow*, 3 ed. McGraw-Hill: Boston, 2003.
16. Anderson JA. *Hypersonic and High-Temperature Gas Dynamics*, 2 ed. AIAA Education Series: Reston, 2006.
17. Sutton GP, Biblarz O. *Rocket Propulsion Elements*, 8 ed. John Wiley & Sons: Hoboken, 2010.
18. Fröhlich A, Popp M, Schmidt G, Thelemann D. Heat transfer characteristics of H2/O2 combustion chambers. *Proceedings of the 29th Joint Propulsion Conference*, Monterrey, USA, 1993; AIAA 93-1826.
19. Habiballah M, Vingert L, Vuillermoz P. Research as a key in the design methodology of liquid-propellant combustion devices. *Journal of Propulsion and Power* 1998; **14**(5): 782-788.
20. Marchi CH, Laroca F, Silva AFC, Hinckel JN. Numerical solutions of flows in rocket engines with regenerative cooling. *Numerical Heat Transfer - Part A* 2004; **45**: 699-717.
21. Barros JEM, Alvim Filho GF, Paglione P., 1990, Study of reactive flow in non-equilibrium through convergent-divergent nozzles (in Portuguese). *Proceedings of the 3rd National Meeting of Thermal Sciences (ENCIT)*, Itapema, Brazil, 1994.
22. Smith TA, Pavli AJ, Kacynski KJ. Comparison of theoretical and experimental thrust performance of a 1030:1 area ratio rocket nozzle at a chamber pressure of 2413 kN/m2 (350 psia). Cleveland, NASA Lewis Research Center, *NASA Technical Paper 2725*, 1987.

23. Svehla RA. Thermodynamic and transport properties for the hydrogen-oxygen system. Cleveland, NASA Lewis Center, *NASA SP-3011*, 1964.
24. Kee RJ, GrCar JF, Smooke MD, Miller JA. A Fortran program for modeling steady laminar one-dimensional premixed flames. Albuquerque, Sandia National Laboratories, *SAND85-8240•UC-401*, 1990.
25. Marchi CH, Araki LK, Laroca F. Evaluation of thermochemical properties and combustion temperatures for LOX/LH2 reaction schemes. *Proceedings of the 26th Iberian Latin-American Congress on Computational Methods in Engineering*, Guarapari, Brazil, 2005.
26. Araki LK, Marchi CH. Numerical solution of an one-dimensional reactive flow in a regeneratively rocket engine nozzle, *Proceedings of the 11th Brazilian Congress of Thermal Sciences and Engineering*, Curitiba, Brazil, 2006.
27. Schneider GE, Zedan M. A modified strongly implicit procedure for the numerical solution of field problems. *Numerical Heat Transfer* 1981; **4**: 1-19.
28. Van Doormaal JP, Raithby GD. Enhancements of the SIMPLE method for predicting incompressible fluid flow. *Numerical Heat Transfer* 1984; **7**: 147-163.
29. Marchi CH, Silva AFC. Multi-dimensional discretization error estimation for convergent apparent order. *Journal of the Brazilian Society of Mechanical Sciences and Engineering* 2005; **27**(4): 432-439.
30. Richardson LF. The approximate numerical solution by finite differences of physical problems involving differential equations, with an application to the stresses in a masonry dam. *Philosophical Transactions of the Royal Society of London – Series A* 1910; **210**: 307-357.
31. Richardson LF, Gaunt JA. The deferred approach to the limit. *Philosophical Transactions of the Royal Society of London – Series A* 1927; **227**: 299-361.
32. Back LH, Massier PF, Gier HL. Comparison of measured and predicted flows through conical supersonic nozzles, with emphasis on the transonic region. *AIAA Journal* 1965; **3**(9): 1606-1614.
33. Incropera FP, DeWITT DP, BERGMAN TL, LAVINE AS. *Fundamentals of Heat and Mass Transfer*, 6 ed, John Wiley & Sons: New York, 2007.
34. Cuffel RF, Back LH, Massier PF. Transonic flow in a supersonic nozzle with small throat radius of curvature. *AIAA Journal* 1969; **7**: 1364-1366.
35. Kliegel JR, Levine JN. Transonic flow in small throat radius of curvature nozzle. *AIAA Journal* 1969; **7**: 1375-1378.
36. Marchi CH, Silva AFC. Unidimensional numerical solution error estimation for convergent apparent order. *Numerical Heat Transfer – Part B* 2002; **42**(2): 167-188.
37. Roache PJ. Discussion: "Factors of safety for Richardson extrapolation" (Xing, T., and Stern, F., 2010, ASME, J. Fluid Eng., 132, p.061403). *Journal of Fluids Engineering* 2011; **133**: 115501.
38. ASME. *Standard for Verification and Validation in Computational Fluid Dynamics and Heat Transfer. ASME V&V 20-2009*. 2009.

Table 1. Chemical reaction schemes implemented in Mach2D 6.0 code.

Model	*L*	*N*	Species	Observations
0	0	3	H_2O, O_2, H_2	Ideal model
1	1	3	H_2O, O_2, H_2	–
2	2	4	H_2O, O_2, H_2, OH	–
3	4	6	H_2O, O_2, H_2, OH, O, H	4 reactions with 3rd body – Barros et al. [21] and Smith et al. [22]
4	4	6	H_2O, O_2, H_2, OH, O, H	4 reactions – Svehla [23]
5	8	6	H_2O, O_2, H_2, OH, O, H	8 reactions (4 with 3rd body) – Barros et al. [21]
7	8	6	H_2O, O_2, H_2, OH, O, H	8 reactions (4 with 3rd body) – Smith et al. [22]
10	6	8	H_2O, O_2, H_2, OH, O, H, HO_2, H_2O_2	4 reactions from model 3 and 2 from Kee et al. [24] – all the reactions including 3rd body
9	18	8	H_2O, O_2, H_2, OH, O, H, HO_2, H_2O_2	18 reactions (5 with 3rd body) – Kee et al. [24]

Table 2. Discharge coefficient for air flow through Back et al. [32] nozzle (720x80 grid, Problem 1).

Case 1:		
Air flow, stagnation pressure of 1.725 MPa, stagnation temperature of 833.33 K, $\gamma = 1.35$.		
Analytical solution by Kliegel and Levine [35]: 0.982020.		
Physical model	UDS	CDS
One-species, constant properties	$0.99 \pm 2\text{x}10^{-2}$ $(p_U \approx 0.93)$	$0.98169 \pm 2\text{x}10^{-5}$ $(p_U \approx 2.74)$
One-species, variable properties	$0.99 \pm 2\text{x}10^{-2}$ $(p_U \approx 0.93)$	$0.98428 \pm 2\text{x}10^{-5}$ $(p_U \approx 2.93)$
Case 2:		
Air flow, stagnation pressure of 482.6 kPa, stagnation temperature of 300 K, $\gamma = 1.40$.		
Analytical solution by Kliegel and Levine [35]: 0.981652		
Experimental value by Cuffel et al. [34]: 0.985		
Physical model	UDS	CDS
One-species, constant properties	$0.99 \pm 2\text{x}10^{-2}$ $(p_U \approx 0.92)$	$0.98140 \pm 2\text{x}10^{-5}$ $(p_U \approx 2.29)$
One-species, variable properties	$0.99 \pm 2\text{x}10^{-2}$ $(p_U \approx 0.92)$	$0.98108 \pm 2\text{x}10^{-5}$ $(p_U \approx 2.28)$

Table 3. Results for C_d, F and I_S for the parabolic nozzle (320x96 grid, Problem 2).

Model	C_d [adim.]	F [N]	I_S [s]
UDS			
One-species, constant properties	$1.01 \pm 2\text{x}10^{-2}$	$1.628\text{x}10^{4} \pm 8\text{x}10^{1}$	$3.45\text{x}10^{2} \pm 5\text{x}10^{0}$
One-species, variable properties	$1.00 \pm 2\text{x}10^{-2}$	$1.635\text{x}10^{4} \pm 8\text{x}10^{1}$	$3.45\text{x}10^{2} \pm 5\text{x}10^{0}$
Frozen Flow – mod. 4	$1.01 \pm 2\text{x}10^{-2}$	$1.621\text{x}10^{4} \pm 9\text{x}10^{1}$	$3.39\text{x}10^{2} \pm 5\text{x}10^{0}$
Frozen Flow – mod. 10	$1.01 \pm 2\text{x}10^{-2}$	$1.621\text{x}10^{4} \pm 8\text{x}10^{1}$	$3.39\text{x}10^{2} \pm 5\text{x}10^{0}$
Equilibrium Flow – mod. 4	$0.98 \pm 1\text{x}10^{-2}$	$1.665\text{x}10^{4} \pm 7\text{x}10^{1}$	$3.56\text{x}10^{2} \pm 5\text{x}10^{0}$
Equilibrium Flow – mod. 10	$0.98 \pm 2\text{x}10^{-2}$	$1.665\text{x}10^{4} \pm 7\text{x}10^{1}$	$3.56\text{x}10^{2} \pm 5\text{x}10^{0}$
Non-equilibrium Flow – mod. 31	$1.06 \pm 2\text{x}10^{-2}$	$1.651\text{x}10^{4} \pm 8\text{x}10^{1}$	$3.27\text{x}10^{2} \pm 4\text{x}10^{0}$
Non-equilibrium Flow – mod. 32	$1.07 \pm 2\text{x}10^{-2}$	$1.654\text{x}10^{4} \pm 8\text{x}10^{1}$	$3.25\text{x}10^{2} \pm 4\text{x}10^{0}$
CDS with deferred correction			
One-species, constant properties	$0.999876 \pm 2\text{x}10^{-6}$	$1.62516\text{x}10^{4} \pm 4\text{x}10^{-1}$	$3.41743\text{x}10^{2} \pm 8\text{x}10^{-3}$
One-species, variable properties	$0.991678 \pm 4\text{x}10^{-6}$	$1.632442\text{x}10^{4} \pm 8\text{x}10^{-2}$	$3.46111\text{x}10^{2} \pm 3\text{x}10^{-3}$
Frozen Flow – mod. 4	$1.000962 \pm 2\text{x}10^{-6}$	$1.61859\text{x}10^{4} \pm 4\text{x}10^{-1}$	$3.39993\text{x}10^{2} \pm 8\text{x}10^{-3}$
Frozen Flow – mod. 10	$1.000970 \pm 2\text{x}10^{-6}$	$1.61860\text{x}10^{4} \pm 4\text{x}10^{-1}$	$3.39991\text{x}10^{2} \pm 8\text{x}10^{-3}$
Equilibrium Flow – mod. 4	$0.9785 \pm 5\text{x}10^{-4}$	$1.6625\text{x}10^{4} \pm 3\text{x}10^{0}$	$3.572\text{x}10^{2} \pm 2\text{x}10^{-1}$
Equilibrium Flow – mod. 10	$0.9785 \pm 5\text{x}10^{-4}$	$1.6625\text{x}10^{4} \pm 3\text{x}10^{0}$	$3.572\text{x}10^{2} \pm 2\text{x}10^{-1}$
Kliegel and Levine [35] – 2D analytical solution for irrotational, one-species, constant properties flow	0.999877	---	---

Table 4. Results for P_{ex}, T_{ex}, u_{ex} and $Y(H_2O)_{ex}$ (at the line symmetry), for the parabolic nozzle (320x96 grid, Problem 2).

Model	P_{ex} [Pa]	T_{ex} [K]	u_{ex} [m/s]	$Y(H_2O)_{ex}$ [adim.]
UDS				
One-species, constant properties	$7.2\text{x}10^{4} \pm 7\text{x}10^{3}$	$1.99\text{x}10^{3} \pm 4\text{x}10^{1}$	$3.03\text{x}10^{3} \pm 5\text{x}10^{1}$	---
One-species, variable properties	$7\text{x}10^{4} \pm 1\text{x}10^{4}$	$2.09\text{x}10^{3} \pm 4\text{x}10^{1}$	$3.06\text{x}10^{3} \pm 6\text{x}10^{1}$	---
Frozen Flow – mod. 4	$6.9\text{x}10^{4} \pm 3\text{x}10^{3}$	$1.92\text{x}10^{3} \pm 3\text{x}10^{1}$	$3.03\text{x}10^{3} \pm 5\text{x}10^{1}$	0.783686
Frozen Flow – mod. 10	$6.9\text{x}10^{4} \pm 2\text{x}10^{3}$	$1.92\text{x}10^{3} \pm 3\text{x}10^{1}$	$3.03\text{x}10^{3} \pm 4\text{x}10^{1}$	0.783539
Equilibrium Flow – mod. 4	$8.3\text{x}10^{4} \pm 3\text{x}10^{3}$	$2.64\text{x}10^{3} \pm 1\text{x}10^{1}$	$3.10\text{x}10^{3} \pm 5\text{x}10^{1}$	$0.902 \pm 2\text{x}10^{-3}$
Equilibrium Flow – mod. 10	$8.3\text{x}10^{4} \pm 2\text{x}10^{3}$	$2.64\text{x}10^{3} \pm 1\text{x}10^{1}$	$3.10\text{x}10^{3} \pm 5\text{x}10^{1}$	$0.902 \pm 2\text{x}10^{-3}$
Non-equilibrium Flow – mod. 31	$7.6\text{x}10^{4} \pm 2\text{x}10^{3}$	$2.06\text{x}10^{3} \pm 3\text{x}10^{1}$	$2.89\text{x}10^{3} \pm 4\text{x}10^{1}$	$0.8614 \pm 4\text{x}10^{-4}$
Non-equilibrium Flow – mod. 32	$7.7\text{x}10^{4} \pm 2\text{x}10^{3}$	$2.07\text{x}10^{3} \pm 2\text{x}10^{1}$	$2.87\text{x}10^{3} \pm 4\text{x}10^{1}$	$0.8794 \pm 6\text{x}10^{-4}$
CDS with deferred correction				
One-species, constant properties	$7.14\text{x}10^{4} \pm 9\text{x}10^{2}$	$1.98\text{x}10^{3} \pm 1\text{x}10^{1}$	$3.04\text{x}10^{3} \pm 2\text{x}10^{1}$	---
One-species, variable properties	$7.34\text{x}10^{4} \pm 9\text{x}10^{2}$	$2.083\text{x}10^{3} \pm 7\text{x}10^{0}$	$3.07\text{x}10^{3} \pm 1\text{x}10^{1}$	---
Frozen Flow – mod. 4	$6.90\text{x}10^{4} \pm 9\text{x}10^{2}$	$1.91\text{x}10^{3} \pm 2\text{x}10^{1}$	$3.04\text{x}10^{3} \pm 5\text{x}10^{1}$	0.783686
Frozen Flow – mod. 10	$6.90\text{x}10^{4} \pm 9\text{x}10^{2}$	$1.91\text{x}10^{3} \pm 2\text{x}10^{1}$	$3.04\text{x}10^{3} \pm 5\text{x}10^{1}$	0.783539
Equilibrium Flow – mod. 4	$8.31\text{x}10^{4} \pm 8\text{x}10^{2}$	$2.6345\text{x}10^{3} \pm 3\text{x}10^{-1}$	$3.113\text{x}10^{3} \pm 5\text{x}10^{0}$	$0.903 \pm 1\text{x}10^{-3}$
Equilibrium Flow – mod. 10	$8.31\text{x}10^{4} \pm 8\text{x}10^{2}$	$2.6347\text{x}10^{3} \pm 3\text{x}10^{-1}$	$3.113\text{x}10^{3} \pm 5\text{x}10^{0}$	$0.903 \pm 1\text{x}10^{-3}$

Figure Captions:

Figure 1. Rocket engine nozzle profiles used for numerical simulations: (a) Geometry from Back et al. [32]; (b) Parabolic geometry.

Figure 2. Pressure distribution through the nozzle for air flow (720x80 control volumes, Problem 1).

Figure 3. Mach number distribution through the nozzle for air flow (720x80 control volumes, Problem 1) in the transonic region.

Figure 4. Comparison of numerical and experimental Mach number distributions in the transonic region (720x80 control volumes, Problem 1). Numerical interpolation schemes: (a) UDS and (b) CDS.

Figure 5. (a) Temperature distribution, for different grid refinements (frozen flow, chemical model 3, CDS with deferred correction) for Problem 1; (b) zoom at the nozzle exit results.

Figure 6. Apparent order for (a) UDS and (b) CDS, frozen flow, model 4, Problem 2.

Figure 7. Error estimate for (a) UDS and (b) CDS for I_S, frozen flow, model 4, Problem 2.

Figure 8. Apparent order obtained for (a) UDS and (b) CDS, equilibrium flow, model 4, Problem 2.

Figure 9. Error estimate for (a) UDS and (b) CDS for I_S, equilibrium flow, model 4, Problem 2.

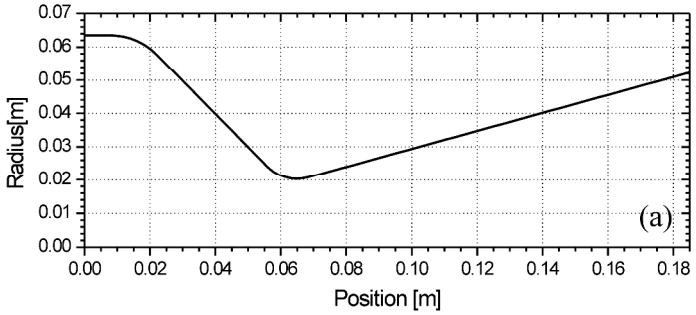

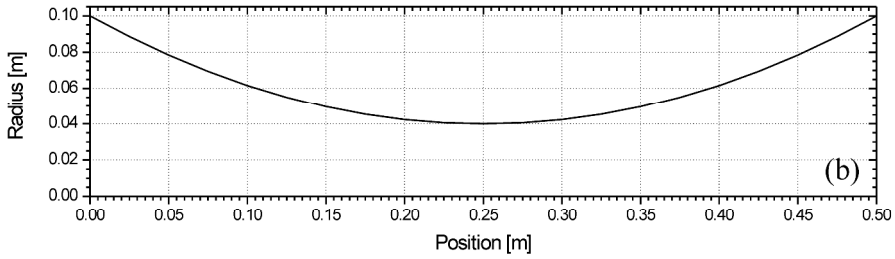

Rocket engine nozzle profiles used for numerical simulations: (a) Geometry from Back et al. [32]; (b) Parabolic geometry.

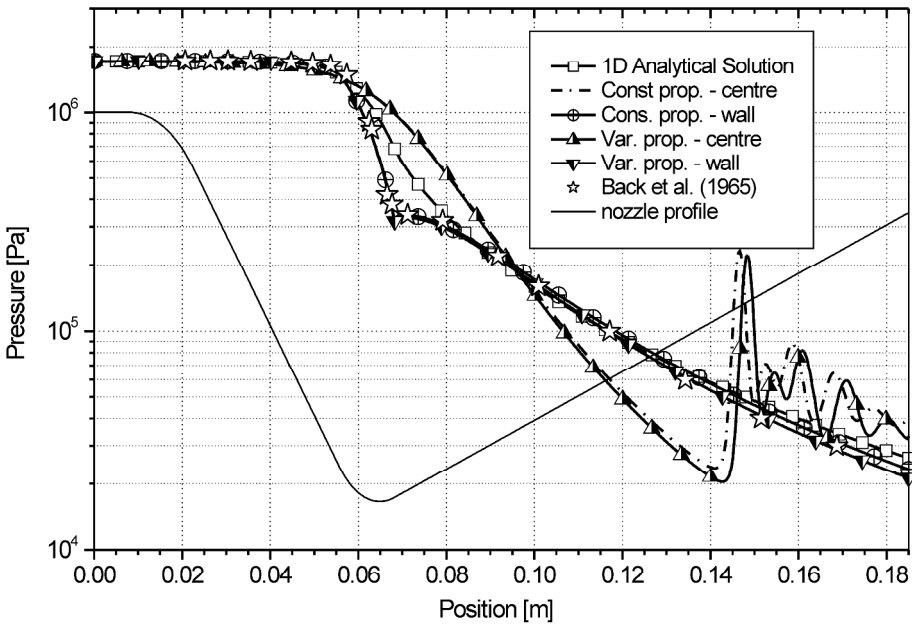

Pressure distribution through the nozzle for air flow (720x80 control volumes, Problem 1).

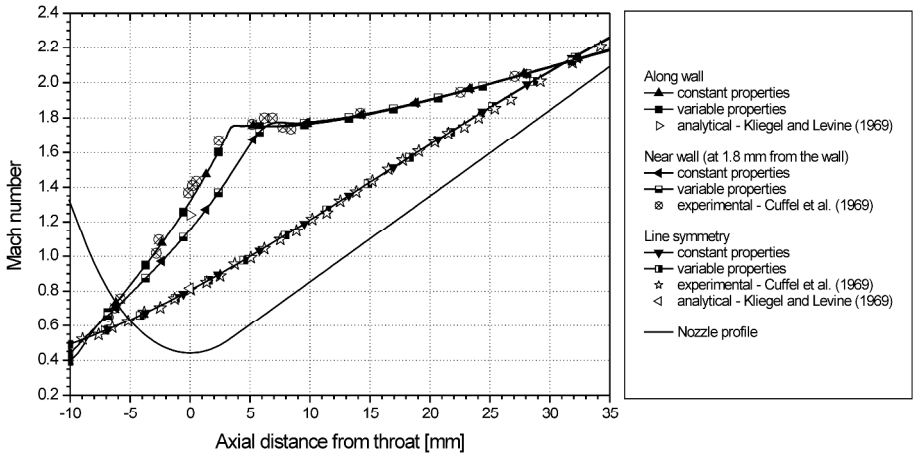

Mach number distribution through the nozzle for air flow (720x80 control volumes, Problem 1) in the transonic region.

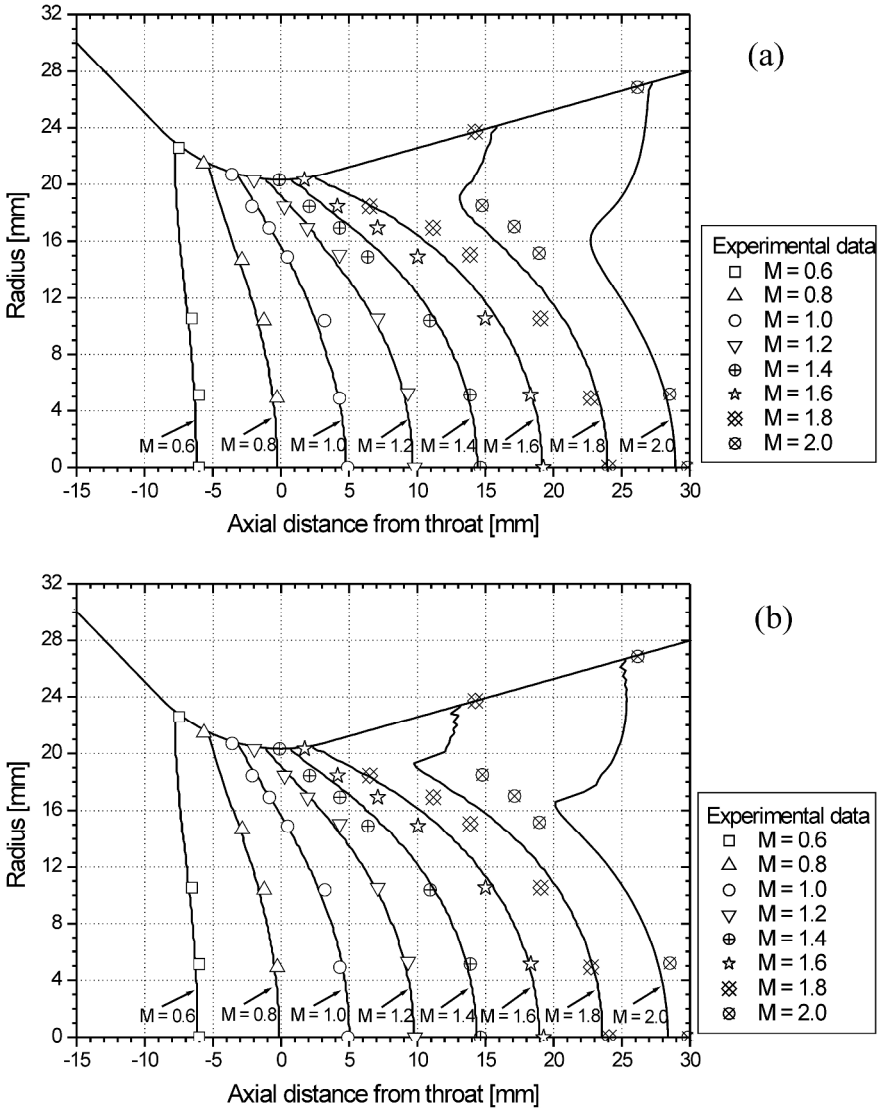

Comparison of numerical and experimental Mach number distributions in the transonic region (720x80 control volumes, Problem 1). Numerical interpolation schemes: (a) UDS and (b) CDS.

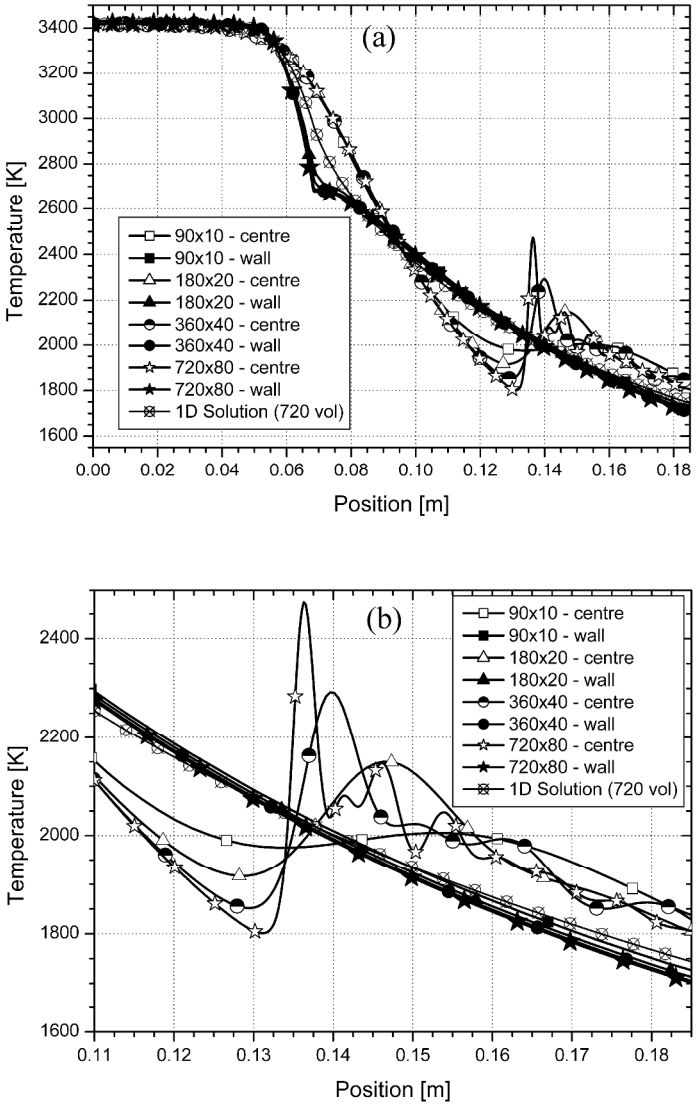

(a) Temperature distribution, for different grid refinements (frozen flow, chemical model 3, CDS with deferred correction) for Problem 1; (b) zoom at the nozzle exit results.

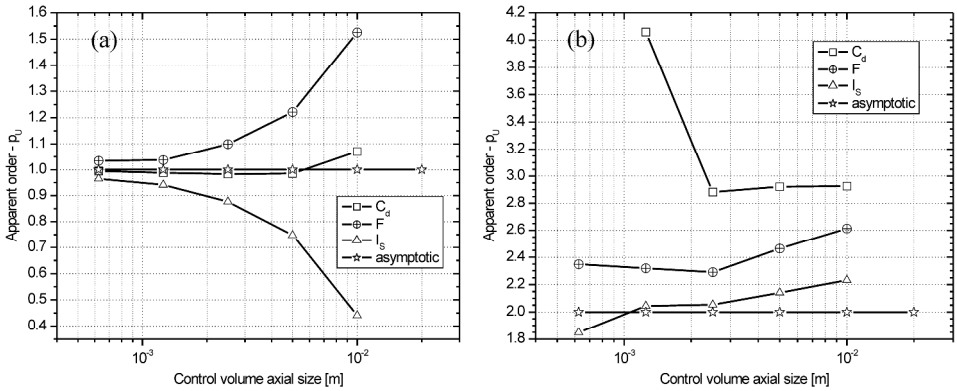

Apparent order for (a) UDS and (b) CDS, frozen flow, model 4, Problem 2.

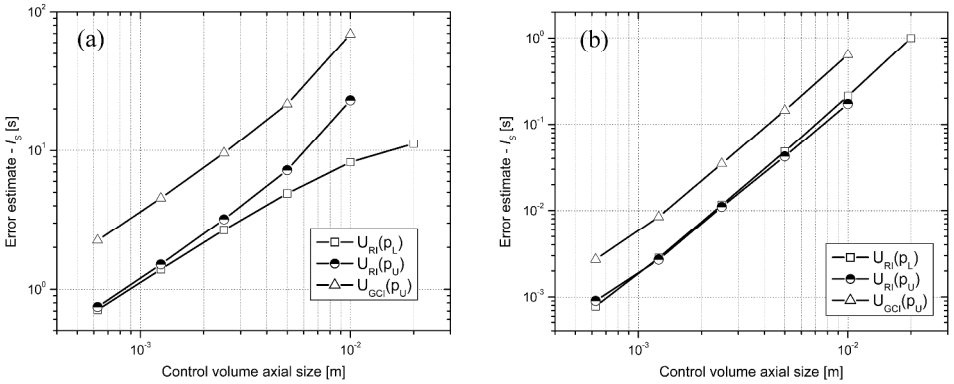

Error estimate for (a) UDS and (b) CDS for IS, frozen flow, model 4, Problem 2.

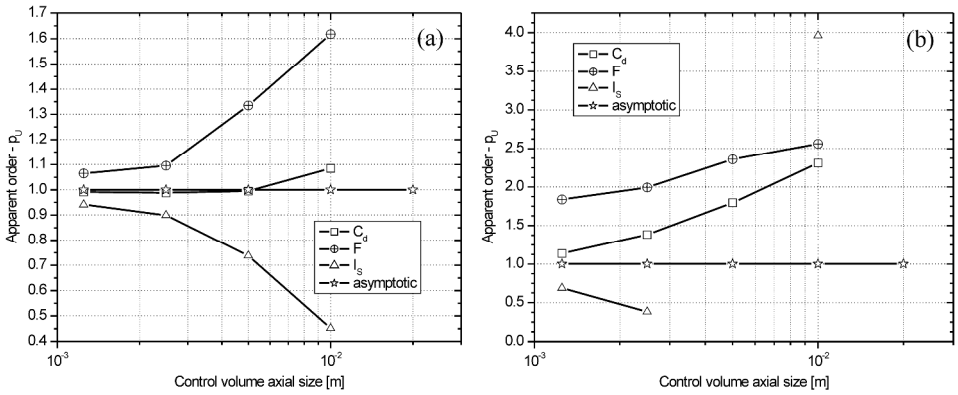

Apparent order obtained for (a) UDS and (b) CDS, equilibrium flow, model 4, Problem 2.

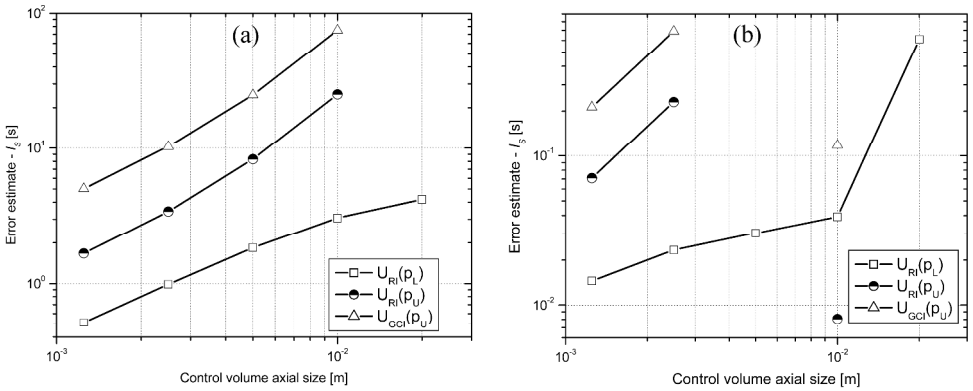

Error estimate for (a) UDS and (b) CDS for IS, equilibrium flow, model 4, Problem 2.